VARIATIONAL ASSIMILATION OF PRECIPITATION DATA AND GRAVITY WAVE ADJUSTMENT

Luc Fillion

Direction de la Recherche en Météorologie, Dorval, Québec

Corresponding author address: Dr. Luc Fillion, *Meteorological Services of Canada, 2121 Voie de Service Nord, Route Transcanadienne, Dorval, Québec, Canada, H9P 1J3. e-mail: Luc.Fillion@ec.gc.ca*

Abstract

The degree of imbalance forced by deep-convection in a three-dimensional variational analysis scheme (3D-Var) is examined. Simulated surface precipitation-rates are used with various degree of errors together with different background atmospheric fields covering a range of forcing from summer to explosive weather regimes. Dynamical imbalances are defined only for the fastest timescales associated to gravity waves and diagnosed according to the Implicit Normal Mode framework. Local measures of ageostrophic perturbations are also considered over rainy areas. Slow time-scale perturbations on internal gravitational modes introduced by convection during 3D-Var are also monitored using temporal evidence of their presence.

It is found that gravity-wave imbalance is introduced early in the minimization process when no balance constraint is imposed (other than the simple local geostrophic constraint used in the background error statistics). Precipitation observations localized over a restricted horizontal domain are sufficient to trigger non-negligeable imbalances. A challenging issue is the introduction of slow time-scale internal modes which significantly differ from those already present in the background trajectory. Whether these oscillations need to be controlled in some ways in order to ensure that the variational adjustment of convective forcing leads to slow time-scales within some neighborhood of those of the background trajectory remains an open question. Traditional normal mode tools as those used in implicit normal mode initialization (especially for the first two internal vertical modes) can be used for such constraining problems in principle. For operational applications, the now widely used digital time-filtering approach presumably would need some extension in order to achieve the same controlling effect on slow time-scales.

1. Introduction

The problem of assimilating surface precipitation in operational data analysis systems is now receiving a considerable attention among the data assimilation community. Among the various candidate for the analysis scheme to assimilate such data, the variational approach receives the most intense consideration but more traditional approaches for such problems, e.g. the nudging method are currently in use at some operational centers (the Met. Office in England for instance, Jones and MacPherson 1997). A model time-tendency approach is also under investigation at the Data Assimilation Office (DAO) at NASA (Hou et al. 2000a,b, 2001). The variational approach offers a coherent consideration of error statistics and a direct use of model operators normally present during a forecast. This approach however is not without serious difficulties at the present time. At the statistical foundation, we still need to clarify the use of appropriate error distribution for modelization and observational contributions. A simple example of this aspect is given in Errico et al. (2000). The importance of model error contribution, especially at the end of the time assimilation window, in a 4D-Var assimilation context presumably also reduces the possible impact of crucial (end time) data needed for improving short-term forecast of precipitation for instance. Many other basic issues like these still need to be addressed before claiming the superiority of the 4D-Var approach over other approaches like those mentioned above in the context of short-term precipitation forecast for instance.

On the other hand, many important and basic properties of the minimization problem and special characteristics of different convective schemes were isolated and clarified in so called 1D-Var precipitation assimilation contexts ; Fillion and Errico (1997, hereafter noted FE), Treadon (1997), Fillion and Mahfouf (2000, hereafter noted FM), Marécal and Mahfouf (2000a,b).

The current state of research on the potential usefulness of the variational apporach for precipitation assimilation is now mainly focused on 3D and 4D contexts. These contexts require carefully designed experiments to clearly exhibit and isolate the source of potential problems that may appear and more importantly, to optimally assimilate such observations. This paper is dedicated to such an attempt ; i.e. clarifying the degree of excitation of gravity waves during 3D-Var assimilation of surface precipitation rates. We deliberately discard unnecessary technical details (that we know from operational experience to have a limited impact) and focus on the desired phenomenon.

The focus of this study is on the examination of extra-tropical gravity wave forcing within the 3D-Var analysis step. A special attention could also be placed on global dynamical balance based on a similar analysis system as the one used here but designed for the whole globe (as the ones used operationally at the Canadian Meteorological Center CMC in Montréal, Canada, the European Center for Medium range Weather Forecasts, ECMWF in Reading, England, Météo-France in Toulouse, France, and the National Center for Environmental Predictions, NCEP in Washington D.C., USA). Results such as those of Lane et al. (2000) (see also their references) for the tropical regions represent a useful background in order to extend their analysis to the data assimilation context. We have deliberately separated the research task on the proper treatment of balance constraint within 3D or 4D-Var in two steps : (1) the diagnosis of imbalance during a multivariate variational analysis of precipitation data involving moist-convection and (2) incorporation of a control term within the variational analysis to penalize departures from reasonable balance known a-priori from theoretical considerations. Considerable work was done by Dr. A. Kasahara and colleagues at CGD/NCAR during the last two decades on diabatic initialization. Their contribution to the problem of variational analysis of precipitation data (in a more restrictive way as used here) and combined treatment of fast gravity-wave noise in the tropics is relevant to our problem (see for instance Kasahara et al. 1996 and the chain of references on their work in their reference section). There is also the Physical Initialization procedure, initiated by Dr. T.N. Krishnamurti and colleagues at Florida State University and further developed by other contributors (see e.g. Krishnamurti et al. 1993). Within this approach (basically nudging), some research work has been done on the balance issues as reported for instance in Kumar (1990). Related, potentially interesting research work was done by Drs. G. Browning and H.O. Kreiss on the Bounded Derivative Initialization theory, and also recently the emergence of their reduced system dynamics for mesoscale applications (see also Thomas and Browning, 2000 for time-stepping issues related to gravity waves). It is at the same time obvious that these previous contributions, which have long been discarded in operational applications, now become very important in order to optimally constrain the analysis step to assimilate precipitation observations. Although this balance issue is by no mean restricted to the assimilation of precipitation data (other conventional data raise similar kind of balance considerations), it forces more the developers of new operational analysis schemes to explicitly consider the influence of moist-physical processes in the analysis step (e.g. moist-convection).

Section 2 describes the forecast model used and the data assimilation procedure. Section 3 describes the results of the examination of gravity wave imbalance for a summer case and an explosive winter case. Section 4 gives a summary and conclusions of the study.

2. The model and data assimilation components

2.1 The model

The model used here is the Mesoscale Adjoint Modeling System (MAMS2) at the National Center for Atmospheric Research (NCAR) described by Errico et al. (1994) including some modifications mentioned below. Other useful details about the original model formulation can be found in Anthes et al. (1987). Basic features are:

Area: Limited area, primitive equation model prescribed in flux form on an Arakawa B-grid with a Lambert conformal mapping.

Boundary conditions: Lateral boundary conditions are formulated using a Davies and Turner (1977) relaxation scheme applied within 5 grid points of the domain's edge.

Time-scheme: The time scheme is split-explicit following Madala (1981) with an Asselin (1972) time filter.

Vertical-coordinate: $\sigma = \frac{(p - p_t)}{(p_s - p_t)}$ where p is pressure, p_t is the model top at 10 mb, p_s is surface pressure. The same definition of vertical-coordinate is used in the GEM (Global Environmental Model, Côté et al. 1998) model used operationally at CMC for regional and global weather forecasting. This has implications for the construction of balanced temperature analysis increments as discussed later.

Vertical grid: The wind components (u,v), temperature (T) and mixing-ratio are defined on 16 equally spaced levels in values of σ. The vertical finite-differencing follows the energy-conserving formulation of the NCAR Community Climate Model (CCM2; Hack et al. 1993).

Boundary-Layer scheme: Stability-independent bulk formulation following Anthes et al. (1987).

Vertical Diffusion: Stability-dependent following Kiehl et al. (1996).

Horizontal Diffusion: Fourth-order scheme with a time-independent coefficient applied to the wind, temperature and mixing-ratio except near the lateral boundaries where diffusion is second order.

Dry convective adjustment: Acts only on temperature with no accompanying mixing of moisture.

Ground-Temperature: The prognostic equation for ground-temperature includes radiative effects modeled identically to those of Anthes et al. (1987), which includes consideration of fractional coverage by three levels of clouds determined simply as a piece-wise linear function of relative humidity.

Large-scale precipitation: Based on a value of 100% relative humidity. Excess moisture is precipitated after approximately accounting for increase in temperature and saturation vapor pressure due to condensation. Values for the specific heat of air and latent heat of evaporation are treated as T-independent for this calculation. No evaporation of precipitation falling below the level of condensation is considred.

Moist convection: Relaxed Arakawa-Schubert (RAS) scheme developed by Moorthi and Suarez (1992), plus a consideration of evaporation of falling precipitation (provided by Moorthi and Suarez) and depth-dependent relaxation time scales. These time scales range betwen 2.5 h for deep clouds to 1h for shallow clouds (here a minimum depth of 100 mb).

2.2 The background fields and simulated data

The background fields used in the experiments reported here were produced from a short-term 6-h forecast from initialized analyses. Those fields come from ECMWF analyses interpolated from 7 pressure levels (100, 200, 300, 500, 700, 850, 1000 hPa) to the 16 equally spaced σ levels of the 3D-Var/MAMS2. The horizontal resolution of ECMWF fields is compatible with a global spherical-harmonic representation with a

triangular truncation at T42. These fields are produced on a Gaussian grid of 128 x 64 mesh points in the zonal and meridional direction respectively. The initialization is performed with an adiabatic first-order implicit normal mode approach (Temperton 1988) and the details of the initialization procedure can be found in Errico et al. (1994) and references. The deepest three vertical modes are initialized using three iterations of the first-order Machenhauer's scheme. The model was run with complete physics at a horizontal resolution of 50 km. There are 65 x 65 grid points in the north-south and east-west directions respectively, giving a horizontal domain of approximately 3200 Km in both horizontal directions. In order to give various estimates of the degree of imbalance caused by the adjustment of convection in this multivariate 3D-Var analysis, a summer case and an explosive winter case were chosen. The summer background fields are valid at 00 UTC, june 17, 1997. The explosive case is the same one as used by FE and the background fields are valid at 0600 UTC, 12 february 1982.

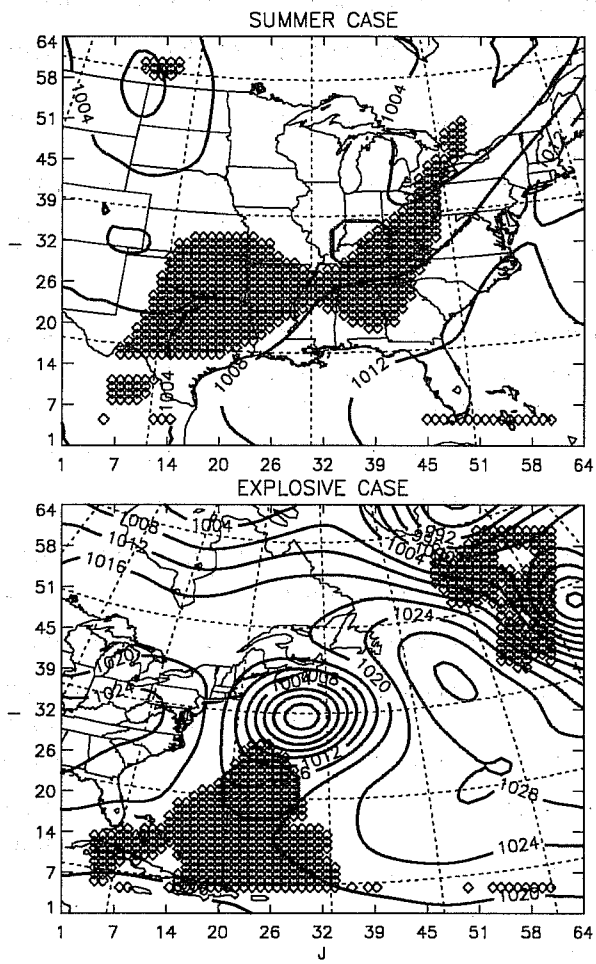

Fig. 1. Mean sea-level pressure for the summer case : 17 june 1997, 00 UTC and explosive winter case : 12 February 1982, 06 UTC. Small circles indicate grid-point locations where the RAS convective scheme produces surface precipitation.

Figure 1 shows the mean sea level pressure of the background fields for both summer and explosive cases. In addition, the grid points where convective precipitation is producing surface precipitation are shown by small diamonds (i.e. the RAS scheme is applied to the temperature, specific-humidity and surface pressure of the background). Also appearing in the figures is the disk to be used when simulating "observed" surface precipitation-rates. Note the clear delimitation of convective points close to the boundaries in fig.1 due to the

absence of convective treatment of grid points within the sponge layer, which is restricted to the five nearest points from the edge of the domain.

The simulation of "observed" surface precipitation-rate data was done using a random perturbation about the background precipitation-rate using a 25% amplitude (uniformly distributed). Once again, as in FE and FM, we do not consider the important aspect for operational assimilation of precipitation data of the so called "convective/non-convective" discrepancy between the background and observation from remote detection (satellite or radar instruments) of surface-precipitation. We recognize that this is definitely one crucial aspect that needs to be examined in future studies. As opposed to the 1D-Var studies of FE and FM, the present three-dimensional context forces a realistic use of the horizontal distribution within the observation disk of the *sign* of the surface rain-rate innovations, i.e. increase or decrease of precipitation. This information was given to us by Dr. Mahfouf and Marecal from ECMWF, and was extracted from their tropical 1D-Var experiments on precipitation assimilation. It is relevant at this point to stress that at the present time, little is known on the statistics of model and observational errors involved in current satellite or radar estimates of surface precipitation-rates.

This crucial aspect of the assimilation problem needs further attention in order to avoid improperly forcing these data into the continuously growing and sensitive data assimilation procedures used at operational NWP centers. The emphasis is placed in this study on the dynamical balance leaving for future studies in realistic operational context the question of the impact on short and medium range forecast.

2.3 The 3D-var Scheme

A simple 3D-Var scheme was developed during the course of this study and designed for limited area models. It is based on many similar assumptions (although less sophisticated) currently in use in major operational centers but is basically a limited-area version rather than global spatial coverage. It is similar to the HIRLAM/ALADIN limited-area 3D-Var formulation (Gustafsson et al. 1999).

The simple approach taken here is to consider data away from the lateral boundaries of the domain (i.e. distant by more than the horizontal correlation scales used in this study, and outside the model relaxation zone, i.e. 5 gridpoints). The analysis is formulated in terms of analysis increments. The problem of incorporating the lateral boundary conditions within the analysis step is generally considered at the present time to be an open question. This aspect, together with the well-posedness of dynamical balance schemes is simply avoided here in order to focus on the balance characteristics of the precipitation assimilation problem. This means here that whenever the model is used to compute time-tendencies, constant lateral boundary conditions are used.

Analysis increments for a given scalar field ξ is represented by its Discrete Fourier-Transform (DFT) :

$$\xi_{mn} = \sum_{j=0}^{N_x-1} \sum_{l=0}^{N_y-1} \xi_{jl} \exp(2\pi imj / N_x) \exp(2\pi inl / N_y),$$

and Inverse Discrete Fourier Transform (IDFT) :

$$\xi_{jl} = \frac{1}{N_x N_y} \sum_{m=0}^{N_x-1} \sum_{n=0}^{N_y-1} \xi_{mn} \exp(-2\pi ijm / N_x) \exp(-2\pi i \ln / N_y).$$

Here, $N_x = N_y = 64$ (the dimension of the inside-mesh in Arakawa B grid).

We introduce the vector $\delta \mathbf{x} = (\delta u, \delta v, \delta T_u, \delta q, \delta p_s)^T$, i.e. gridpoint analysis increments. If u and v are the components of the wind vector along the axes of the coordinate system, then the wind images U and V are given by

$$U = \frac{u}{m} \quad ; \quad V = \frac{v}{m} \quad ; \quad m = \frac{\sin \varsigma_1}{\sin \phi} \left[\frac{\tan \varsigma/2}{\tan \varsigma_1/2} \right]^{0.716} \qquad \varsigma_1 = 30^o \ , \varsigma \ \textit{is colatitude} \ .$$

Using the Helmholtz decomposition theorem, we have the relations

$$U = -\frac{\partial \psi}{\partial y} + \frac{\partial \chi}{\partial x} \quad ; \quad V = \frac{\partial \psi}{\partial x} + \frac{\partial \chi}{\partial y} \qquad (2.1),$$

where ψ, χ are the streamfunction and velocity potential of the wind field.

From the streamfunction analysis increment $\delta\psi$, we define a "balanced" mass increment δP as $\delta P = f \, \delta \psi$.

We define a balanced temperature increment $\delta T_b = \mathbf{V} \delta P$, where the matrix $\mathbf{V}$ acts on vertical profiles of δP. The latter is usually obtained from linear regression of forecast differences for such quantities (e.g. Derber and Bouttier, 1999, Gauthier et al. 1998). Such a procedure was unavailable to us since no sequential data assimilation procedure is availble at NCAR. We took advantage here of the fact that the CMC model's coordinate is the same as the one used here. There is however a difference between the *number* of vertical levels (28 versus 16 for GEM and MAMS2 resp.) and *vertical distribution* of levels between the two models (variable as compared to uniform vertical distribution for GEM and MAMS2 resp.). This is a limiting aspect of the current study in the sense that this may limit the full transposition of our balance diagnostic results to operational centers which make use of regressions directly from their analysis system. Similar and sometimes more sophisticated regression procedures are used to define their balanced components of mass (this the case for ECMWF for instance). We believe however that although some dynamical balance details may vary, most of our analysis results to be presented here should transpose reasonably well to current 3D-Var operational practice and be considered useful when precipitation data will (or is) considered. Our approach is to use the CMC 28-levels regression matrix, noted $\mathbf{V}_H$, and use interpolation operators between the two high (H) and low (L) resolution vertical grids (i.e. GEM versus MAMS2) such that

$$\delta T_b = \mathbf{V} \, \delta P = \Pi_L \, \mathbf{V}_H \, \Pi_H \, \delta P \qquad (2.2)$$

Figure 2 shows the result of 3D-Var for a single observation at 500 hPa. The vertical structure of T_b (solid-line) indicates that our approach produces reasonable results in terms of known vertical background error correlations for temperature. Also, the much weaker amplitude of T_u (dashed-line) indicates the proper behavior of the analysis and reflects simply the smaller error variance ascribed to this analysis variable as compared to the effective T_b error variance. Note however that our modelling of the vertical correlation of T_u is not standard (as compared to operational centers using a similar approach) since it uses the Gaussian

assumption that does not allow negative lobes. This could be another limitation of our study for useful transposition to operational practice but we believe the impact of this difference on balance diagnostics is small. The reason for this is twofold : the use of only surface-precipitation data here and the fact that the convection scheme acts to change the vertical profiles of T and q much more below 700 hPa. The net result of this is that the vertical correlation of T_u which is relevant during the minimization is its local structure which is well approximated by the Gaussian assumption.

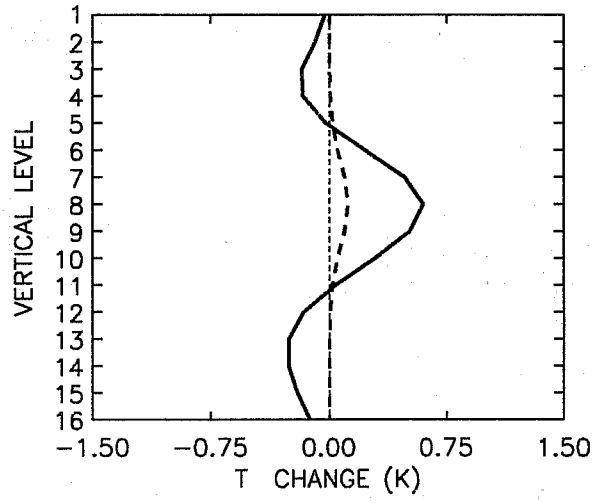

Fig. 2. Balanced (solid line) and unbalanced (dashed-line) temperature increments resulting from the 3D-Var assimilation of one single temperature observation at 500 hPa.

Combining the horizontal and vertical transforms above, the unbalanced part of temperature at each horizontal gridpoints is obtained as

$$\delta T_u = \delta T - \delta T_b = \delta T - f\,\mathbf{V}\delta\psi \quad (2.3)$$

where f is the local Coriolis parameter value. This transform basically describes an operator **B** which acts on temperature and streamfunction increments, leaving the other parts of the state-vector unchanged.

Background-error correlations are assumed to be homogeneous and isotropic in the horizontal. The gridpoint model used here is a Gaussian function with horizontal correlation scales allowed to vary in the vertical. Their horizontal spectral representations (spectral densities) follows Yaglom (1987), ch. 4, Daley (1991), ch. 4. This approach is used for all analysis variables which are the streamfunction (ψ), velocity potential (χ), unbalanced temperature (T_u), specific-humidity (q) and surface pressure (p_s). The resulting correlations in Fourier/Vertical physical space are block-diagonal for each analysis variables. This is expressed as

$$J_b = \frac{1}{2}\,\delta\xi^{\mathrm{T}}\,\mathbf{C}^{-1}\,\delta\xi\,;\;\; \delta\xi = \mathbf{F}\,\mathbf{D}^{-1}\,\mathbf{B}\,\delta\mathbf{x}\,;\;\mathbf{D} = \mathit{diag}\left[\sigma_\psi, \sigma_\chi, \sigma_{T_u}, \sigma_q, \sigma_{p_s}\right] \quad (2.4),$$

where **F** represents a DFT in the horizontal.

A further eigen-decomposition of the vertical matrices for each horizontal waves of the Fourier representation in the horizontal completely diagonalizes the background term. More precisely, (ignoring the horizontal mode notation for simplicity), we get :

$$J_b = \frac{1}{2}\,\delta\xi^{\mathrm{T}}\mathbf{C}^{-1}\,\delta\xi = \frac{1}{2}\delta\xi^{\mathrm{T}}(\mathbf{E}\Lambda\mathbf{E}^{-1})^{-1}\,\delta\xi$$
$$= \frac{1}{2}\delta\xi^{\mathrm{T}}(\mathbf{E}\Lambda^{-1}\mathbf{E}^{-1})\,\delta\xi = \frac{1}{2}(\delta\xi^{\mathrm{T}}\mathbf{E}\Lambda^{-1/2})\,(\Lambda^{-1/2}\mathbf{E}^{-1}\delta\xi)$$
$$= \frac{1}{2}\,\delta\mathbf{k}^{\mathrm{T}}\,\delta\mathbf{k} \quad ; \quad \text{where} \quad \delta\mathbf{k} \equiv \Lambda^{-1/2}\mathbf{E}^{-1}\delta\xi \quad .$$

The vertical correlation matrices being real-symmetric, we have $\mathbf{E}^{\mathrm{T}}=\mathbf{E}^{-1}$ and the desired transformation is:

$$\delta\mathbf{k} = \Lambda^{-1/2}\,\mathbf{E}^{\mathrm{T}}\,\mathbf{F}\,\mathbf{D}^{-1}\,\mathbf{B}\,\delta\mathbf{x} \qquad (2.5) \quad .$$

This defines the control vector for the minimization. In pratice, the initial minimization point is chosen to be the background state and for such cases, during the minimization, we only need to recover the grid-point analysis increment $\delta\mathbf{x}$ from $\delta\mathbf{k}$, i.e. we use explicitly

$$\delta\mathbf{x} = \mathbf{L}\,\delta\mathbf{k} = \mathbf{B}^{1/2}\,\mathbf{D}\;\mathbf{F}^{-1}\,\mathbf{E}\,\Lambda^{1/2}\,\delta\mathbf{k} \qquad (2.6) \quad .$$

Here, $\mathbf{B}^{1/2}$ simply means obtaining δT_b from (2.2) and then δT from (2.3). In terms of this control vector, the full functional to be minimized and its gradient are :

$$J = \frac{1}{2}\delta\mathbf{k}^{\mathrm{T}}\delta\mathbf{k} + \frac{1}{2}(H(\mathbf{L}\delta\mathbf{k}))^{\mathrm{T}}\mathbf{R}^{-1}(H(\mathbf{L}\delta\mathbf{k}))\,,$$

$$\nabla J = \delta\mathbf{k} + \mathbf{L}^{*}\mathbf{H}^{\mathrm{T}}\mathbf{R}^{-1}(H(\mathbf{L}\delta\mathbf{k}))\,.$$

The adjoint operator $\mathbf{L}^{*}$ is just the transpose of the matrix representation of the operator $\mathbf{L}$ (as defined in (2.6)) except for an additional operator following $\mathbf{F}^{-1}$ in order to take account of the change of norm from complex to real vector representations. We use the M1QN3 minimization code of Gilbert and Lemaréchal (1989).

The observation operator H for precipitation-rates at the surface is defined as in FE where the RAS moist-convective scheme is used.

The background error statistics are as follows. The vertical variation of the standard deviations of the error on the unbalanced part of temperature, i.e. σ_{T_u}, is specified as in FM but interpolated from the 31 ECMWF levels to the 16 MAMS levels. There is no horizontal variation of σ_{T_u} however over our limited-area analysis domain. The values for $\sigma_{\psi},\sigma_{\chi}$ are obtained from the model coordinate 3D-Var analysis system operational at CMC since june 14, 2000 via Daley's partitioning from the wind components (ref. Daley 1991, sec 5.2.27), i.e.

$$\sigma_{\psi} = \sqrt{1-\nu^2}\;L_{\psi}\,\sigma_u \;; \quad \sigma_{\chi_u} = \nu\,L_{\chi_u}\,\sigma_u \quad .$$

No horizontal variation on the analysis domain of these quantities is considered. The parameter ν^2 is allowed to vary in the range $0 \le \nu^2 \le 0.1$, i.e. from purely rotational wind analysis increments to a level of divergent wind increment similar to innovations typically observed when computed against radiosonde

network (Hollingsworth and Lönnberg 1986). Values above 0.1 are not considered here but their impact on the covariance structure is discussed in Daley (1985). Although the 3D-Var code developed here has the flexibility to accomodate vertical variation of horizontal correlation scales for each analysis variables, we decided to keep them fixed in our numerical experiments. There are basically two reasons for doing this. First, no sequential data assimilation cycle was available to us in order to derive such statistics, as in Derber and Bouttier (1999). We could attempt to model this vertical variation according to what is currently available at operational centers. However, based on this information, it appears that no significant variation is apparent below 500 hPa. In addition, FM showed that most of the vertical adjustment of temperature and moisture during the adjustment of moist -convection is done in the lower troposphere for the majority of convective schemes examined. For these two reasons, the following fixed horizontal scales were used in the experiments to be presented in the next section :

$$L_\psi = L_\chi = L_{T_u} = L_q = 150\ Km\ .$$

Finally, the vertical variation of the error standard-deviation for specific-humidity is also extracted from the CMC system. Table 1 gives the explicit values used in this study for the vertical variation of the above statistics where a vertical interpolation was used to bring CMC's 28 vertical levels to MAMS 16 levels.

Level	σ_ψ (m^2s^{-2})	σ_{T_u} (K)	σ_q (g/Kg)
1	3.25×10^6	0.61	0.87×10^{-2}
2	3.09×10^6	0.65	0.11×10^{-1}
3	2.71×10^6	0.68	0.15×10^{-1}
4	2.31×10^6	0.64	0.28×10^{-1}
5	2.02×10^6	0.63	0.59×10^{-1}
6	1.81×10^6	0.63	0.11
7	1.62×10^6	0.63	0.17
8	1.51×10^6	0.62	0.24
9	1.48×10^6	0.62	0.31
10	1.44×10^6	0.61	0.39
11	1.41×10^6	0.61	0.50
12	1.38×10^6	0.66	0.64
13	1.34×10^6	0.70	0.83
14	1.31×10^6	0.69	1.02
15	1.30×10^6	0.73	1.07
16	1.30×10^6	0.80	1.15

Table 1

2.4 Balance diagnostics

We use Temperton's (1988) Implicit Normal Mode approach (see also Juvanon du Vachat 1986, Bourke and McGregor 1983) to characterize the imbalance developed during the course of the unconstrained 3D-Var analysis, i.e. when no explicit balancing term is added to the functional presented previously. This diagnostic involves the computation of the value BAL for each vertical modes diagnosed. This quantity is defined as

$$BAL = \iint_D \left\{ (\delta_t \phi)_G^2 + \Phi \left[(\delta_t U)_G^2 + (\delta_t V)_G^2 \right] \right\} dx\, dy \ ,$$

where the equivalent geopotential depth Φ and the time tendencies of wind-images U and V are for a given vertical mode (ref. Temperton and Roch 1991) among those treated by the diagnostic (first three deepest modes here). The integral is performed over the horizontal analysis domain. The need to complement this

diagnostic will be discussed as we proceed with the results in the next section. It is important to stress here that Machenhauer's first-order balance condition is well monitored by the BAL quantity and tends towards zero for each vertical modes if the balancing scheme converges (Temperton 1988). In addition, as demonstrated by Errico (1989a,b), the full model (including physical processes) as used here develops a balance which satisfies accurately this Machenhauer's condition ; i.e, the balance is basically an adiabatic one for the deepest gravitational modes. For shallowest (slower) internal gravitational modes, Machenhauer's balance (including highest order ones) is less representative of the model's own balance where these modes have non-negligeable time-tendencies. Our interest here lies in the diagnostic of imbalance on the deepest three vertical modes caused by the adjustment of convection during 3D-Var.

The sequence of steps to compute the BAL quantity, for each vertical modes, is :

1. Run the adiabatic MAMS2 model for one forward timestep to obtain the coupled tendencies $(\delta_t(p*u),\delta_t(p*v),\delta_t(p*T),\delta_t(p^*))$, where $p^* \equiv (p_s - p_T)$, p_s is surface pressure, p_T a prescribed, x-y independent, top pressure.

2. Go from

   $$(\delta_t(p*u),\delta_t(p*v),\delta_t(p*T),\delta_t(p^*)) \text{ to } (\delta_t U,\delta_t V,\delta_t \varphi) ,$$

   where U,V are wind-images as defined above and φ is an auxiliary variable called pseudo-geopotential defined as

   $$\varphi = \overline{p}_{vm}\left(\phi + R\,\overline{T}\ln\frac{\sigma p^* + p_T}{\overline{p}_{vm}}\right)$$

   where $\overline{T}$, $\overline{p}_{vm}$ are time and space independent p* and T about which the linearization is performed (to compute the vertical normal modes), ϕ is geopotential obtained from the hydrostatic equation.

3. Go from $(\delta_t U,\delta_t V,\delta_t \varphi)$ to $(\delta_t \zeta,\delta_t D,\delta_t \varphi)$ using the vorticity and divergence operators of the model in terms of wind-images.

4. Couple the tendencies $(\delta_t \zeta,\delta_t \varphi)$ to form the ageostrophic vorticity tendency $\delta_t \eta$, where

   $$\eta \equiv \zeta - \frac{m^2}{f_o}\nabla^2\varphi$$

5. Solve for ΔD : $-m^2\nabla^2(\Delta D) + \frac{f_o^2}{\Phi}(\Delta D) = \frac{1}{\Phi} f_o(\delta_t \eta)$

6. Compute $(\delta_t\phi)_G$: $(\delta_t\phi)_G = m^2\,\Phi\,\nabla^2(\Delta\chi) = \Phi\,(\Delta D)$

7. Get $(\delta\chi)_G$: $\delta_t(\chi)_G = \delta_t(\chi)$

8. Compute $(\delta_t\psi)_G$: $\nabla^2(\delta_t\psi)_G = m^{-2}(f\,\Delta D)$

9. Compute $(\delta_t U)_G,(\delta_t V)_G$, from $(\delta_t\psi)_G,(\delta_t\chi)_G$

10. Compute a value of BAL for each vertical modes as defined above.

In addition to the BAL value, we introduce a local value giving an indication of mass convergence forced by the multivariate analysis and related to the balance criteria mentioned above. This value is defined here as

$$LAB = \iint_{Disk} (\delta_t D)^2 \, dx \, dy \, .$$

Since one constraint of the Implicit Normal Mode Initialization approach (INMI, Machenhauer's scheme), is defined in terms of the vanishing of the time-tendency of the divergence over the model's horizontal domain, for each vertical mode considered, the value LAB would tend to zero as the INMI scheme is iterated. In order to avoid the dominance over the rainy area assimilated of the exterior disk contribution to the above horizontal area integration, the LAB value is introduced. The meaning of LAB will loosely be used as a Limited-Area Balance but this latter word should be used with great care since it only gives a partial portrait of the imbalance in a general context. In addition, this LAB value helps to visualize the extent to which the mass convergence, so important in the triggering and maintenance of moist-convection, evolves locally in time and can be used to better appreciate its potential effect on convection. In other words, we are specifically interested here in the temporal evolution of the LAB value for each vertical modes. The time-tendency of the linearized potential vorticity appearing as an additional component of the full characterization of the first-order balance condition (stated above) has also been monitored. It was observed that this component adds nothing new over the temporal behavior of the LAB value and has a very similar behavior whether in forecast or 3D-Var analysis mode. For this reason, we did not add this contribution in our local diagnostic. Moreover, the BAL value is a bit restrictive in our context since it sums the contribution of time-tendencies over the whole model integration domain and (as mentioned above) tends to hide the local imbalance created during 3D-Var due to the dominance of the ouside disk contribution to the integral (especially for internal vertical modes). For this reason, we mostly discuss results of our experiments in terms of the LAB value.

3. Results

3.1 1D-Var versus 3D-Var

We present a first experiment to give an idea of the difference of results that can be obtained when surface precipitation data are assimilated point by point as with 1D-Var and the case where all available surface precipitation data are used in the disk (see Fig. 1, summer case). Figure 3 shows the results of these two types of variational analysis in terms of the reduction of the norm of the gradient, surface rain-rate at the center point of the disk, and the resulting specific-humidity and temperature analysis increments (solid and dashed lines respectively).

As is the case in numerous 1D-Var analyses performed in FM for instance, it is eeen that the reduction of the norm of the gradient is significant (4 orders of magnitudes) and the convergence is fast (3 iterations). On the other hand, the results from 3D-Var show that the reduction of the norm of the gradient is more difficult (only one order of magnitude after 20 iterations). It is also interesting to note that due to the overall interaction with other convective points in the disk (via the 3D background coupling), the surface rain-rate is *decreased* during the first two iterations and then gradually increased to match more closely the observed rain-rate. Also important to note is the significant difference in vertical structure of the analysis increments for 1D and 3D-Var respectively at the center point of the disk for T and q.

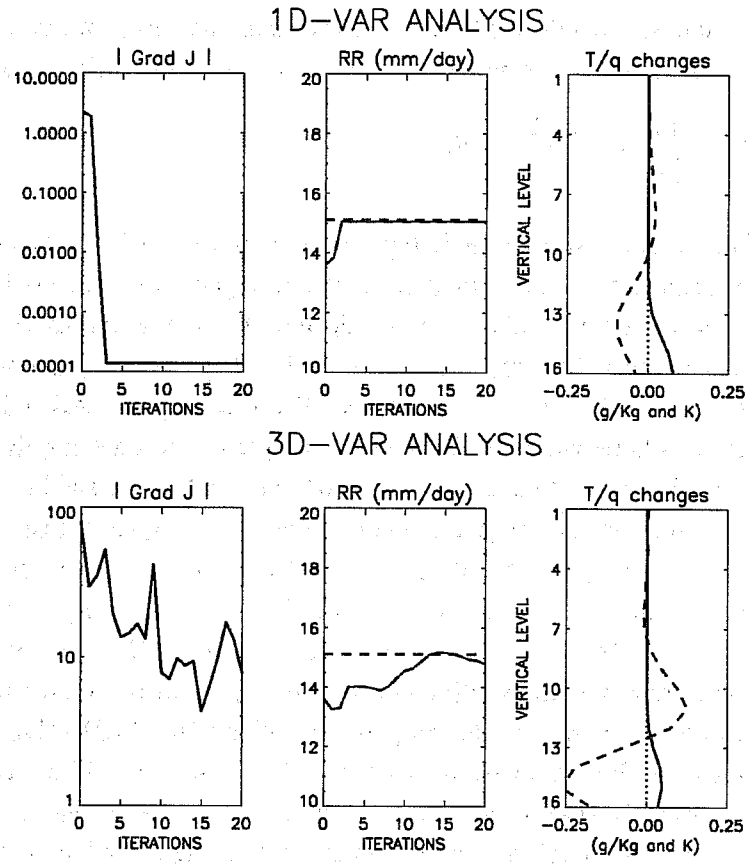

Fig. 3. Results of 1D-Var and 3D-Var analyses using the summer case. For the 1D-Var analysis, only the rain-rate at the center of the disk in Fig.1 is assimilated. For the 3D-Var analysis, all rain-rate observations within the disk are being assimilated.

3.2 Summer case

We now turn to the examination of the 3D-Var analyses and especially in terms of gravity waves triggering. The first case examined is the summer case presented in Fig.1. The results are presented in Fig. 4. First, as mentioned previously, the reduction of the norm of the gradient is only one order of magnitude after 20 iterations. To give a global measure of the adjustment of surface rain-rate, we computed the linear correlation coefficient over the observation disk of the logarithm of the analysis rain-rate and the observed rain-rate for each iteration during the minimization. It is seen that a gradual adjustment towards observations is accomplished (not 100% though !) and almost stationary after 10 iterations in spite of the slight but continued reduction of the norm of the gradient after 10 iterations. In order to give an idea of the rate of convergence in terms of amplitude of the analysis increments, we show in the third panel on the right, the euclidean norm of the analysis increments for T and q for each vertical levels over the observation disk for the first five iterations (not labeled in the figure).

The gravity wave (GW) triggering is now discussed. The first panel on the left (second line) shows the behavior of the LAB value defined previously for the external vertical mode. It is worth mentioning how this was computed practically. At every iteration of the minimization, the analysis increments of mass, wind, moisture and surface pressure are added to the background state to form the current analysis fields. These fields are defined on their respective grids following Arakawa's B-grid and this is done consistently during the minimization. Then, the model is integrated for one forward timestep. The following steps are described

in the previous section to compute balance diagnostics. Note that this approach is consistent with INMI approach following Temperton and Roch (1991).

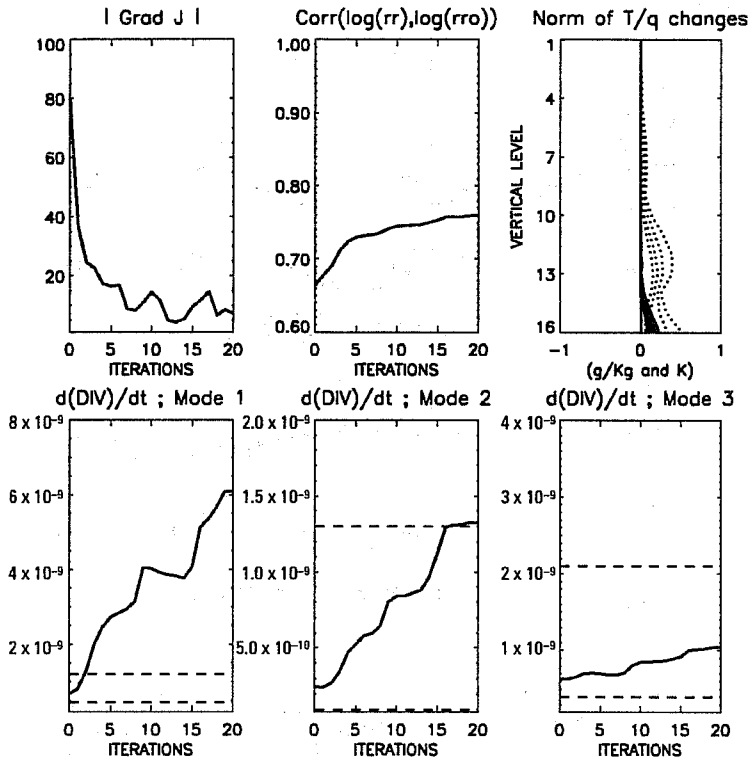

Fig. 4. Results of 3D-Var analysis using the summer case. The norm of T/q changes is computed at each vertical level and over the observation disk. Values of LAB defined in section 2 are given in lower panels for the first three vertical normal modes. Solid lines in these lower panels are for the LAB value at each iterations of 3D-Var. The dashed lines in each panels indicate the extremum values of LAB, computed during the 12h background trajectory and represent the natural forcing of these modes in a 12 h forecast starting from the balanced background state.

The solid line shows how the LAB value is affected for the external mode. A gradual increase is observed during the minimization, indicating a forcing of external GW structure by the adjustment of convection to force precipitation according to the available information of surface precipitation. The degree of this dynamical imbalance must be compared against some measure however. This is done by comparing the natural variability of this LAB value when the model is integrated for 12h starting from the balanced background state. The maximal and minimal values of this quantity have been retained and plotted as the two dashed lines in figure 4. It is seen that the level of imbalance on this external mode is presumably enough to excite external GW modes and be seen for instance by following the time trace of surface pressure at a grid point located inside the disk. Before showing this, we note the additional fact that based on the two other panels respectively for the first and second internal vertical modes, the degree of excitation of the first internal mode is seen to become more important during the last ten iterations but remains within the variability of the background values. The second internal mode being weakly forced.

To judge of the temporal behavior of the resulting analysis, the model is integrated for 12h from the 3D-Var analysis fields and compared against the temporal behavior of the background for the same period of time. Figure 5 shows the time traces of surface-pressure (top panel), divergence at 700 hPa (middle panel) and vertical motion at 700 hPa (lower panel). The behavior of the surface-pressure for the analysis case is

consistent with the external mode diagnosis of fig. 4. The introduction of a distinct internal mode behavior between the analysis and background is apparent in the lower two panels as can be judged from the significant 6-8 h time period.

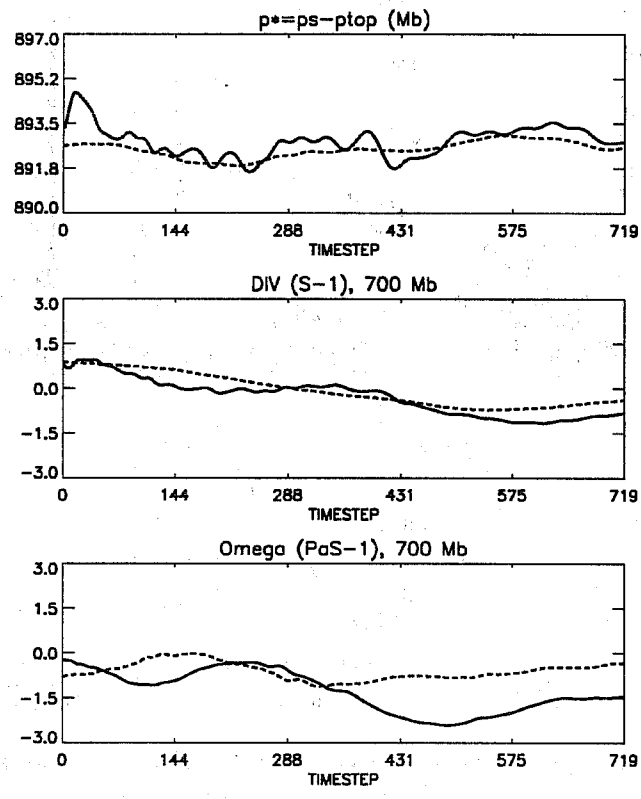

Fig. 5. Time traces of surface-pressure (top panel), 700 hPa divergence (middle panel) and vertical motion at 700 hPa (lower panel) for 12h model integration. Solid line is for the forecast using 3D-Var analysis fields, dashed line is for the forecast using the background state (referred to as the background trajectory in the text).

3.3 Explosive winter case

Similar experiments were performed with an explosive winter case. This case is the same one as used by FE and the background fields are valid at 0600 UTC, 12 february 1982. Figure 6 shows that the rate of convergence of 3D-Var is a bit better than the summer case and reach almost two orders of magnitude reduction of the norm of the gradient within 20 iterations. The structure of the norm of the analysis increments of T and q is converging as fast as the summer case but we note less internal structure in the vertical profiles. This is consistent with the panels of the time tendency below for the first two internal modes where we see a weak forcing of internal vertical scales during the first half of the minimization (first 10 iterations). Note however that the amplitude of the internal mode forcing is stronger both for the background trajectory and the 3D-Var analysis as compared to the summer case. The first panel below for the time tendency of the barotropic mode shows a significant forcing for this mode by 3D-Var and significantly exceeds the natural variability present in the background trajectory. Figure 7 shows the temporal behavior of the same diagnostic quantity used for the summer case. It is clear that there is still a prominent 6-8 h period oscillation present in the forecast done with the 3D-Var analysis as compared to the background trajectory. This appears to be related to a transient oscillation since this amplitude disappear after 12h of integration. Note also that this temporal behavior is not simply due to the passage of the cold

front since this structure of convection was already present in the background state and 3D-Var only enhanced the amplitude of this convective activity based on rain-rate observations. It is clear however that this forcing of convection through 3D-Var results in a transient oscillation.

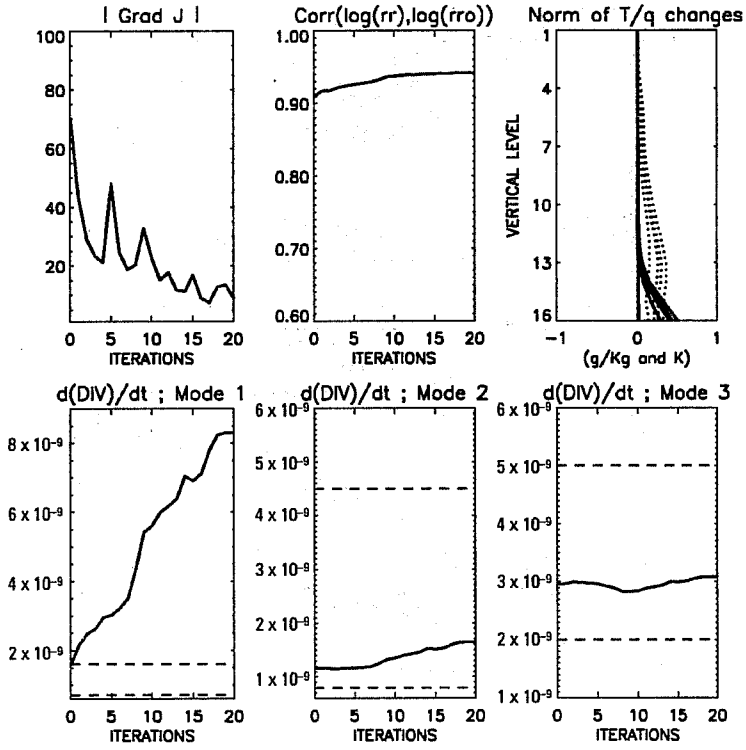

Fig. 6. As in Fig. 4 except for the explosive winter case.

Finally we note that the degree of the fast external mode imbalance is not perceptible very far after the beginning of the forecast (1 or 2 hours) and leaves the disk area with a slow time evolution very similar to the background trajectory. Other experiments performed (results not shown) showed that this region of the explosive case does not exhibit sustained oscillations that can be preceptible by this simple time trace of the surface pressure. This is not caused by a limitation of the LAB quantity as compared to the BAL quantity for the external mode since we explicitly examined the behavior of the BAL value during the 3D-Var minimization and observed a similar increase as the LAB value (one order of magnitude larger after 20 iterations of 3D-Var). The results here simply show that there is a limitation to use the balance diagnostics such as those used here in a static mode since it tells nothing on the rapidity of dissipation of the barotropic gravity mode energy during the model integration; a behavior that is really what is needed during sequential data assimilation rather than a static estimate of the degree of forcing of the fast modes. This philosophy being based on the idea that the background state needs to be balanced in a data assimilation system. With this respect, if the dissipation of the fast vertical gravity waves is done on a time scale of the order or smaller than the sequential assimilation period (typically 6h), then these modes in such cases (as applies here with the explosive case) do not represent a serious nuisance. This would definitely not be the case for a 1h sequential data assimilation procedure however.

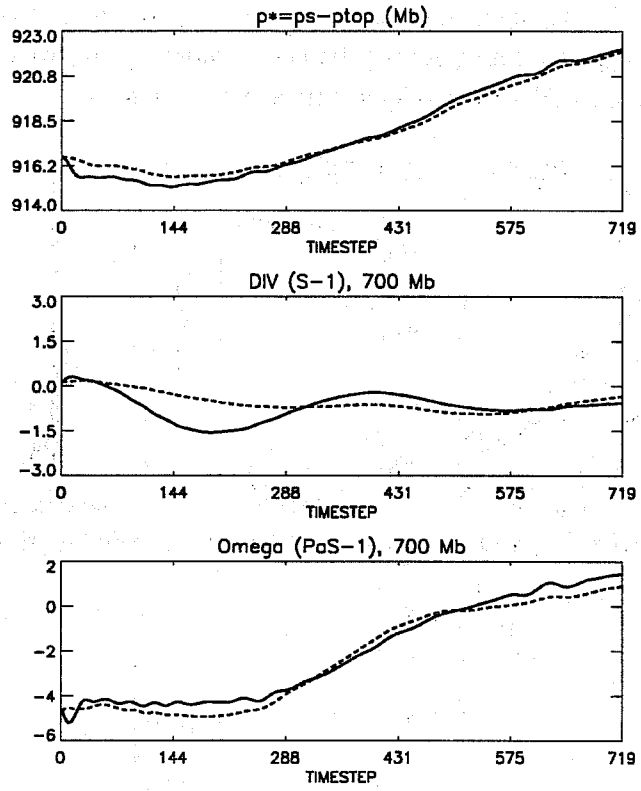

Fig. 7. As in Fig. 5 except for the explosive winter case.

4. Summary

This paper has shown that the 3D-Var assimilation of surface precipitation-rate observations can lead to significant fast (external) and slow (internal) gravity waves. This being the case in a context close to state of the art 3D-Var assimilation schemes for operational purposes around the world. It remains in the future to examine the effect of using an explicit control of the amplitude of the gravity mode tendencies in the 3D-Var analysis step on the nature of the adjustment of convection. Controlling the fast external gravity waves is now efficiently done using normal mode techniques or digital filtering in time. Controlling the amount of slow (internal) gravity modes can also be done as an explicit constraint using normal mode characterizations but appears more difficult to achieve with the digital filtering approach. In particular, it was shown here with a summer case and an explosive winter case that the 3D-Var analysis triggers internal modes which seem to appear as transient oscillations that significantly differ with the background trajectory. The degree of retention of the time tendencies of the gravity modes on various vertical scales needs to be quantified in order to avoid transient oscillations but also to allow a proper adjustment of convection over rainy areas. These features represent essential issues to be clarified before operational applications and will form the subject of a following study. It would be beneficial to the operational data assimilation community if similar experiments as those reported here could be duplicated by advanced operational data assimilation centers.

Acknowledgements

The author wishes to thank the members of the Global Dynamics Section at NCAR and especially Drs. Joseph Tribbia and Ron Errico for their hospitality during a one year visit of the author. This research was partially funded by the United State Weather Research Program (USWRP). This work has largely benefitted from the MAMS2 system built by Dr. Errico and Kevin Raeder at NCAR and their help on how to use it. Useful comments from Drs. John Derber, Jim Purser, and Russel Treadon at NCEP and Dale Barker at

MMM/NCAR on early results of this research are acknowledged. Dr. Jean-Francois Mahfouf at ECMWF helped in the internal review process of this paper at MRB.

References

Anthes, R.A., E.-Y. Hsie, and Y.-H Kuo, 1987: Description of the Penn State/NCAR Mesoscale Model Version 4 (MM4). NCAR Tech. Note, NCAR/TN-282+STR. 66 pp. [Avaliable from the National Center for Atmospheric Research, P.O. Box 3000, Boulder, CO 80307, U.S.A.]

Asselin, R., 1972: Frequency filter for time integration. *Mon. Wea. Rev.*, **100**, 487-490.

Bourke, W., and J.L. McGregor, 1983: A nonlinear vertical mode initialization scheme for a limited area prediction model. *Mon. Wea. Rev.*, **111**, 2285-2297.

Browning, G.L., H.-O. Kreiss, 1997: The Role of Gravity Waves in Slowly Varying in Time Mesoscale Motions. *J. Atmos. Sci.*, **54**, 1166-1184.

Côté, J., S. Gravel, A. Méthot, A. Patoine, M. Roch, and A. Staniforth, 1998: The operational CMC-MRB Global Environmental Multiscale (GEM) model : Part I - Design considerations and formulation. *Mon. Wea. Rev.*, **126**, 1373-1395.

Daley, 1985 : The analysis of synoptic scale divergence by a statistical interpolation procedure. *Mon. Wea. Rev.*, **113**, 1066-1079.

_____, 1991: *Atmospheric Data Analysis*. Cambridge University Press, Cambridge, 457 pp.

Davies, H.C. and R.E. Turner, 1977 : Updating prediction models by dynamical relaxation : An examination of the technique. *Quart. J. Roy. Meteor. Soc.* **103**, 225-245.

Derber, J., and F. Bouttier, 1999: A Reformulation of the Background Error Covariance in the ECMWF Global Data Assimilation System. *Tellus*, **51A**, 195-221.

Errico, R.M., K. Raeder, and T. Vukicevic, 1994: Mesoscale Adjoint Modelling System Version I. NCAR Tech Note NCAR/TN-410+IA,214 pp. [Avaliable from the National Center for Atmospheric Research, P.O. Box 3000, Boulder, CO 80307, U.S.A.]

_____, 1989a: The Forcing of Gravitational Modes by Condensational Heating. *Mon. Wea. Rev.*, **117**, 2734-2752.

_____, 1989b: An Analysis of Dynamical Balance in a Mesoscale Model. *Mon. Wea. Rev.*, **118**, 558-572.

_____, L. Fillion, D. Nychka, and Z.-Q. Lu, 2000: Some Statistical Considerations associated with the Data Assimilation of Precipitation Observations. *Quart. J. Roy. Met. Soc.*, **126A**, 339-359.

Fillion, L., and R.M. Errico, 1997: Variational Assimilation of Precipitation Data Using Moist Convective Parameterization Schemes : A 1D-Var Study. *Mon. Wea. Rev.*, **125**, 2917-2942.

_____, and J.-F. Mahfouf, 2000: Coupling of Moist-Convective and Stratiform Precipitation Processes for Variational Data Assimilation. *Mon. Wea. Rev.*, **128**, 109-124.

Gauthier, P., M. Buehner and L. Fillion, 1998: Background-error statistics modelling in a 3D variational data assimilation scheme : estimation and impact on the analyses. *Proceedings of the ECMWF Workshop on diagnosis of data assimilation systems*, 2-4 Nov., Reading, England. Available from the European Centre for Medium-Range Weather Forecasts, Shinfield Park, Reading RG2 9AX, UK.

Gilbert , J.C., and C. Lemaréchal, 1989: Some numerical experiments with variable-storage quasi-Newton algorithms. *Math. Programming*, **45**, 407-435.

Gustafsson, N., S. Hörnquist, M. Lindskog, L. Berre, B. Navascués, S. Thorsteinsson, X.-Y. Huang, K.S. Mogensen, and J. Rantakokko, 1999 : Three-dimensional variational data assimilation for a high resolution limited area model (HIRLAM). Technical Report, 40, January 1999. [Available from HIRLAM 4 Project, c /o Met Éireann, Glasnevin Hill, Dublin 9, Ireland].

Hack, J.J., B.A. Boville, B.P. Briegleb, J.T. Kiehl, P.J. Rasch, and D.L. Williamson, 1993: NCAR Technical Note, NCAR/TN-382+STR, 107pp. [Available from the National Center for Atmospheric Research, P.O. Box 3000, Boulder CO 80307-3000].

Hollingsworth, T., and P. Lönnberg, 1986: The statistical structure of short-range forecast errors as determined from radiosonde data. Part I : The wind field. *Tellus*, **38A**, 111-136.

Hou, A. Y., D. Ledvina, A. da Silva, S. Zhang, J. Joiner, R. Atlas, G. Huffman, and C. Kummerow, 2000: Assimilation of SSM/I derived surface rainfall and total precipitable water for improving the GEOS analysis for climate studies. *Mon. Wea. Rev.*, **128**, 509-537.

_____, S. Zhang , A. da Silva, W. Olson, 2000: Improving assimilated global datasets using TMI rainfall and columnar moisture observations. *J. of Climate*, **13**, 4180-4195.

_____, S. Zhang , A. da Silva, W. Olson, C. Kummerow, and J. Simpson, 2001: Improving global analysis and short-range forecast using rainfall and moisture observations derived from TRMM and SSM/I passive microwave sensors. *Bulletin of Amer. Meteor. Soc.*, **82**, 659-680..

Jones, C.D., and B. MacPherson, 1997 : A latent heat nudging scheme for the assimilation of precipitation data into an operational mesoscale model. *Meteor. Applic.*, **4**, 269-277.

Juvanon du Vachat, R., 1986: A general formulation of normal modes for limited-area models : applications to initialization. *Mon. Wea. Rev.*, **114**, 2478-2487.

Marécal, V. and J.-F. Mahfouf, 2000a: Variational retrieval of temperature and humidity profiles from TRMM precipitation data. *Mon. Wea. Rev.*, **128**, 3853-3866.

_____, and J.-F. Mahfouf, 2000b: Four dimensional variational assimilation of total column water vapour in rainy areas. ECMWF Technical Memorendum, no 314. [Available from the European Centre for Medium-Range Weather Forecasts, Shinfield Park, Reading RG2 9AX, UK].

Kasahara, A., J.-I. Tsutsui, and H. Hirakuchi, 1996: Inversion Methods of Three Cumulus Parameterizations for Diabatic Initialization of a Tropical Cyclone Model. *Mon. Wea. Rev.*, **124**, 2304-2321.

Kiehl, J.T., J.J. Hack, G.B. Bonan, B.A. Boville, B.P. Briegleb, D.L. Williamson, P.J. Rasch, 1996: Description of the NCAR Community Climate Model (CCM3). NCAR Tech Note NCAR/TN-420+STR, 152pp. [Available from the National Center for Atmospheric Research, P.O. Box 3000, Boulder CO 80307-3000].

Krishnamurti, T.N., H.S. Bedi, and K. Ingles, 1993: Physical Initialization Using SSM/I Rain-Rates. *Tellus*, **45A**, 247-269.

Kumar, A., 1990: Generalized Dynamic Normal Mode Initialization. PhD. Thesis. Florida State University. FSU Report no. 90-4, april 1990. [Available from the Department of Meteorology, Florida State University, Tallahassee, Florida, USA, 32306].

Lane, T. P., M. J. Reeder, and T.L. Clark, 2001 : Numerical Modeling of Gravity Wave Generation by Deep Tropical Convection. *J. Atmos. Sci.*, **58**, 1249-1274..

Madala, R. V., 1981: Efficient time integration schemes for atmosphere and ocean models. Finite-difference techniques for vectorized fluid dynamics calculations, D.L. Book, Ed., Springer, 56-74.

Moorthi, S. and M.J. Suarez, 1992: Relaxed Arakawa-Schubert : a parameterization of moist convection for general circulation models. *Mon. Wea. Rev.*, **120**, 978-1002.

Temperton, C., 1988 : Implicit Normal Mode Initialization, *Mon. Wea. Rev.*, **116**, 1013-1031.

_____, and M. Roch, 1991: Implicit Normal Mode Initialization for an Operational Regional Model, *Mon. Wea. Rev.*, **119**, 667-677.

Thomas, S.J. and G.L. Browning, 2000: The accuracy and Efficiency of Semi-Implicit Time-Stepping for Mesoscale Storm Dynamics. Submitted for publication to J. Atmos. Sci.

Treadon, R.E., 1997 : Assimilation of satellite derived precipitation estimates within the NCEP GDAS. PhD. Thesis. The Florida State Iniversity. [Available from the author at NCEP].

Yaglom, A.M., 1987: *Correlation Theory of Stationary and Related Random Functions I, Basic Results.* Springer Series in Statistics, Springer-Verlag, New-York, 526 pp.